Cholesterol Dependent Recruitment of di22:6-PC by a G Protein-Coupled Receptor into Lateral Domains

Alla Polozova and Burton J. Litman
Laboratory of Membrane Biochemistry and Biophysics, National Institute on Alcohol Abuse and Alcoholism, National Institutes of Health, Rockville, Maryland 20852 USA

ABSTRACT Bovine rhodopsin was reconstituted into mixtures of didocosahexaenoylphosphatidylcholine (di22:6-PC), dipalmitoylphosphatidylcholine (di16:0-PC), *sn*-1-palmitoyl-*sn*-2-docosahexaenoylphosphatidylcholine (16:0, 22:6-PC) and cholesterol. Rhodopsin denaturation was examined by using high-sensitivity differential scanning calorimetry. The unfolding temperature was increased at lower levels of lipid unsaturation, but the highest temperature was detected for native disk membranes: di22:6-PC $<$ 16:0,22:6-PC $<$ di16:0,18:1-PC $<$ native disks. The incorporation of 30 mol% of cholesterol resulted in 2–4°C increase of denaturation temperature in all reconstituted systems examined. From the analysis of van't Hoff's and calorimetric enthalpies, it was concluded that the presence of cholesterol in di22:6-PC-containing bilayers induces a level of cooperativity in rhodopsin unfolding. Fluorescence resonance energy transfer (FRET), using lipids labeled at the headgroup with pyrene (Py) as donors and rhodopsin retinal group as acceptor of fluorescence, was used to study rhodopsin association with lipids. Higher FRET efficiencies detected for di22:6-PE-Py, compared to di16:0-PE-Py, in mixed di22:6-PC–di16:0-PC–cholesterol bilayers, indicate preferential segregation of rhodopsin with polyunsaturated lipids. The effective range of the rhodopsin–lipid interactions facilitating cluster formation exceeds two adjacent lipid layers. In similar mixed bilayers containing no cholesterol, cluster formation was absent at temperatures above lipid phase transition, indicating a crucial role of cholesterol in microdomain formation.

INTRODUCTION

Biological membranes carry out numerous functions vital for cell survival. Their complexity arises not only from their vast number of components, but also from sophisticated multilevel organization. The original fluid mosaic model of biological membranes proposed in the pioneering work of Singer and Nicholson (1972) does not account for high levels of organizational complexity. Due to a rapidly accumulating body of evidence, it is widely acknowledged now, that most cellular membranes have highly specialized domains enriched with certain lipids and proteins (Brown and London 1998; Christensen et al., 1999; Ferretti et al., 1999; Fredrichson and Kurzchalia, 1998; Harder et al., 1998; Hooper, 1999; Hwang et al., 1998; Keller et al., 1998; Kinnunen et al., 1994; Masserini et al., 1999; Varma and Mayor, 1998; Welti and Glaser, 1994; Williams et al., 1998; Zuvic-Butorac et al., 1999).

It is also clear that lipids play a very active role in organizing biological membranes, modulating membrane protein function, and mediating the formation of functional domains (Mouritsen, 1998). The attractive forces facilitating segregation of membrane components into clusters range from electrostatic interactions, arising mostly from the lipid headgroup area, to weak Van der Waals and steric interactions, occurring in the interfacial and hydrophobic intramembrane areas. It was shown both theoretically and experimentally that hydrophobic mismatch, spontaneous curvature, and differences in lipid phase transitions can cause spontaneous lipid–protein and lipid-mediated protein association (Dumas et al., 1997; Marsh, 1995; Mouritsen, 1998). However, these studies were performed on saturated lipids, and do not account for interactions involving unsaturated lipid acyl chains. In particular, polyunsaturated lipids present in many biological membranes are of significant functional importance. For example, neuronal and retinal tissues are highly enriched in lipids containing polyunsaturated 22:6n-3 acyl chains (Salem, 1989). It was established previously that the functional activity of the visual pigment rhodopsin, a G protein-coupled receptor and the major protein of retinal rod outer segment disk membrane, is significantly affected by the lipid acyl chain unsaturation (Litman and Mitchell, 1996; Mitchell et al., 1992). The extent of formation of metarhodopsin II, the G protein-activating form of rhodopsin, was drastically enhanced in the presence of polyunsaturated lipids. The highest values of metarhodopsin I–metarhodopsin II equilibrium constant, K_{eq}, approaching the values of K_{eq} measured for the native disk membranes, were obtained for di22:6-PC-containing samples (Litman and Mitchell, 1996). However, on a mole percent basis, the native disk membrane contains only 25% of dipolyunsaturated di22:6n-3 lipids, whereas there are approximately 63% of mixed-chain *sn*-1-saturated and *sn*-2-polyunsaturated lipids (Miljanich et al., 1979), 10% of

Received for publication 14 February 2000 and in final form 24 July 2000.

Address reprint requests to Burton J. Litman, Laboratory of Membrane Biochemistry and Biophysics, NIAAA, National Institutes of Health, 12420 Parklawn Dr., Rockville, MD 20852. Tel.: 301-594-3608; Fax: 301-594-0035; E-mail: litman@helix.nih.gov.

Abbreviations used: di22:6-PC, didocosahexaenoylphosphatidylcholine; di16:0-PC, dipalmitoylphosphatidylcholine; 16:0,22:6-PC, palmitoyl-docosahexaenoylphosphatidylcholine; PE, phosphatidylethanolamine; Py, pyrene; DSC, differential scanning calorimetry, FRET, fluorescence resonance energy transfer.

0006-3495/00/11/2632/12 $2.00

disaturated (di16:0 or di18:0) lipids and 12–14% of cholesterol (Anderson et al., 1979; Stone et al., 1979). It was suggested that, in the native membranes, there is a lateral domain organization facilitating a high level of rhodopsin activity and, at the same time, maintaining the bulk bilayer stability and integrity (Litman and Mitchell, 1996; Mitchell et al., 1998).

The goal of this study was to isolate the effects of lipid acyl chain unsaturation on the organization of membranes containing rhodopsin. For this reason, we chose phosphatidylcholine as a typical bilayer-forming lipid and varied the acyl chain composition, and presence of cholesterol, in several sets of reconstitution experiments. To evaluate the influence of bulk bilayer properties, we examined the thermal unfolding of rhodopsin reconstituted into phosphatidylcholine liposomes with different unsaturation levels. To analyze the "fine" features of membrane organization, we used fluorescence resonance energy transfer (FRET) approach utilizing pyrene lipid-specific probes (Fig. 1) as donors and rhodopsin as acceptor of fluorescence. Due to the relatively short, in the 10^{-8}–10^{-7}-sec timescale, lifetimes of the excited state of fluorophores, FRET is one of the best techniques available to reveal the smallest, nano-size membrane domains.

EXPERIMENTAL PROCEDURES

Sample preparation

All phospholipids and Py-labeled lipid probes were purchased from Avanti Polar Lipids (Alabaster, AL). Cholesterol was obtained from Calbiochem (La Jolla, CA). HPLC, used as a measure of lipid purity, indicated no detectable contamination. All polyunsaturated lipid-containing samples were handled in argon-filled glove boxes to prevent the lipid oxidation. All operations involving rhodopsin were performed in dark rooms, using night-vision goggles. Stock solutions of lipids in chloroform were mixed in glass test tubes. The appropriate type of Py-labeled lipid probe was added at typically 1:100 probe/lipid molar ratio (at this probe/lipid ratio the concentration of probe in the membrane was well below the self-quenching threshold). Chloroform was evaporated under a stream of nitrogen, then the lipids were redissolved in cyclohexane, quickly frozen in dry ice, and lyophilized using a high-vacuum oil pump for 2–4 hrs. The resulting dry powder was dissolved in 10 mM PIPES buffer (pH = 7) containing 50 μM DTPA and a sufficient amount of octyl glycoside (OG) to solubilize the lipid.

Rod outer segment discs from bovine retinas were solubilized in OG, and rhodopsin was purified using concanavalin A (Pharmacia Biotech, Piscataway, NJ) affinity chromatography, according to the previously described procedure (Litman, 1982). Solubilized lipid was mixed with purified rhodopsin at molar ratios ranging from 1000:1 to 100:1, and proteoliposomes were prepared using a modified dilution reconstitution method (Jackson and Litman, 1985). Briefly, the OG-solubilized lipid–rhodopsin mixture was added drop-wise into a detergent-free portion of PIPES buffer at constant stirring. Upon dilution, the final concentration of OG in the sample was reduced to 10 mM, well below the solubilization limit. The diluted samples were loaded into 15-ml-capacity Slide-A-Lyser dialysis cassettes (Pierce Chemical Company, Rockford, IL) and dialyzed for 14–24 hrs at 4°C against at least 50-fold excess of PIPES buffer containing 3 g/l of detergent-absorbing SM-2 Bio-Beads (Bio-Rad Laboratories, Hercules, CA). Under these conditions, the OG concentration was quickly reduced to less than 10 μM, after $<$2 hrs of dialysis, as was established by anthrone assay (Spiro, 1966). After the dialysis, the samples were collected, assayed for lipid and protein concentrations, and used in fluorescence experiments. For DSC experiments, samples were concentrated up to 0.5–1 mg/ml rhodopsin using Amicon microconcentrator (Beverly, MA)

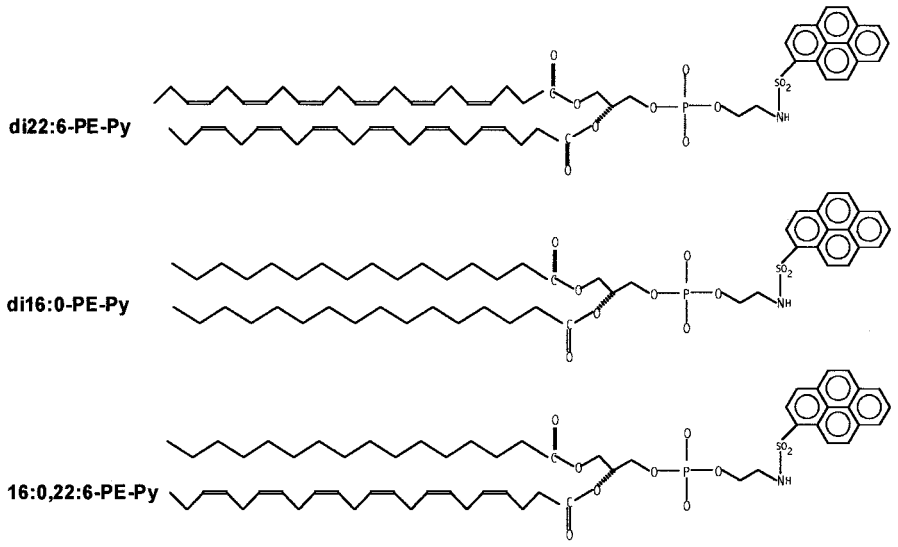

FIGURE 1 Pyrene-labeled lipids

equipped with YM 30 membranes. Final lipid concentration in samples was determined using Phospholipids B assay (Wako Chemicals GmbH, Neuss, Germany). Rhodopsin concentration was evaluated by measuring the difference in absorption at 500 nm between dark-adapted and light-exposed samples. In addition to that, a protein D_C assay (Bio-Rad Laboratories), using OG-solubilized rhodopsin stock solution as a standard, was performed on all samples. Results of absorption measurements and protein-D_C assay were found to be in good agreement with $<5\%$ deviation.

Fluorescence measurements

Steady-state experiments

Steady-state fluorescence measurements were performed using PTI LS100 fluorometer (Photon Technology International, Inc, South Brunswick, NJ) in 4-ml teflon-stoppered cuvettes. All rhodopsin-containing samples were handled in the dark using night-vision goggles. Samples were loaded into the cuvettes and sealed under argon in the argon-filled glove box and transferred into the thermostated fluorometer cell holder equipped with magnetic stirrer. Samples were allowed to equilibrate first at the temperature above the highest T_m of lipids used (50°C) for at least 15 min and than at the temperature of the experiment for at least 30 min. Excitation and emission slits were set at 2 nm and the flash lamp operating at 100 flashes/sec was used as an excitation light source. The difference in Py emission intensity between first and second emission scans due to partial rhodopsin bleaching and Py photobleaching by excitation light was $<5\%$. FRET efficiency for each sample was evaluated as $E = 1 - (I/I_o)$, where I_o is the emission intensity of Py in the absence, and I is the emission intensity in the presence of acceptor. The emission intensity of donor (Py) was measured at 380 nm. The I_o value was measured in the control liposomes containing no rhodopsin.

Time-resolved measurements

Fluorescence lifetime and anisotropy decay measurements of PE-Py probes were performed with a K2 multifrequency cross-correlation phase fluorometer (ISS, Urbana, IL). Excitation at 351 nm was provided by an Innova 307 argon ion laser (Coherent, Santa Clara, CA). Lifetime and differential polarization data were acquired using decay acquisition software from ISS. For lifetime measurements, 12 modulation frequencies were used, logarithmically spaced from 0.5 to 100 MHz. At each frequency, data were accumulated until the standard deviation of the phase and modulation ratio were below 0.2° and 0.004, respectively, and these values were used as the standard deviation for the measured phase and modulation ratio in all analyses.

Differential scanning calorimetry

CSC 6100 Nano-scan II calorimeter (Calorimetry Sciences Corporation, Provo, UT) was used to perform rhodopsin denaturation experiments. Samples were loaded into the calorimeter cells in the dark and sealed under the stream of argon. All scans were performed at 1°C/min scanning rate, experimental curves were processed and analyzed with Cp-Calc 2.1 software.

Sucrose density gradient centrifugation analysis

To ensure that rhodopsin was distributed homogeneously among all liposomes in the process of reconstitution, we performed a sucrose gradient centrifugation analysis of proteoliposome composition. It was performed according to a previously described procedure (Jackson and Litman, 1982). An aliquot of proteoliposomes was layered on top of 1–50% (w/w) continuous sucrose gradient and centrifuged using SW-41 rotor (Beckman, Fullerton, CA) at 30,000 rpm for 6 hrs. The position of resulting bands was observed under a dim red light. The bands were carefully collected using a Pasteur pipette, and analyzed for protein and lipid composition by protein D_C assay (Bio-Rad Laboratories) and Phospholipids B assay (Wako Chemicals GmbH).

For this experiment, we chose samples containing di22:6-PC, di16:0-PC, and cholesterol at 3:7:3 molar ratio, because this set of samples showed a significant difference in the FRET efficiency between the two lipid-specific fluorescent probes. In the process of centrifugation, the liposomes containing 0.5 mol% rhodopsin formed a single band at 19% sucrose. In contrast, protein-free liposomes in the control sample settled at 11% sucrose level. The analysis of protein and lipid content of proteoliposome-containing band confirmed that the liposome composition was uniform and consistent with the starting ratio of lipids. There is no separation of protein from the lipid material during centrifugation: 0.48 ± 0.02 and 0.46 ± 0.01 mol% of rhodopsin was in the samples before centrifugation and in the collected band subsequently. Therefore, rapid dilution reconstitution procedure gives rise to a homogeneous population of proteoliposomes with evenly distributed rhodopsin, even in the case of more complex lipid composition, which is in good agreement with previous findings (Jackson and Litman, 1982).

RESULTS

Unfolding of reconstituted rhodopsin

To reveal the effect of acyl chains on the stability of rhodopsin, we examined the unfolding of this protein reconstituted into phosphatidylcholine liposomes containing lipids of different unsaturation levels. In all dark-adapted samples of reconstituted rhodopsin, a single thermal transition was observed (Fig. 2, *curve 1*). The shape and position

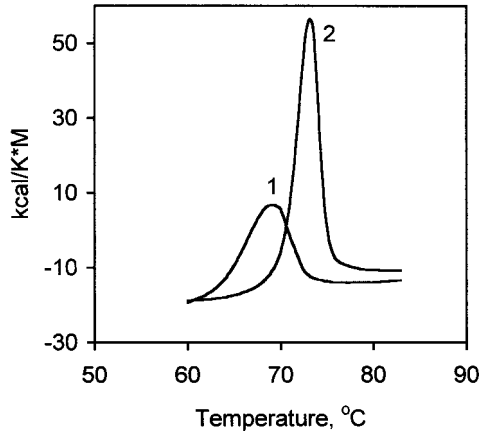

FIGURE 2 Example of rhodopsin denaturation endotherms: *curve 1*, rhodopsin reconstituted into di22:6-PC/cholesterol (10:3) liposomes; *curve 2*, rhodopsin in native disks. Scanning rate = 1 K/min.

of thermal transition curves in reconstituted samples look similar to thermal unfolding of rhodopsin in native membranes (Fig. 2, *curve 2*), and are in good agreement with the previously published data on denaturation of this protein in ROS disks (Miljanich et al., 1985; Shnyrov and Berman; 1988, Khan et al., 1991). Parameters of thermal denaturation curves are summarized in Table 1. It is clear that an increase in lipid unsaturation level results in a decrease of the unfolding temperature: 16:0,18:1-PC > 16:0,22:6-PC > di22:6-PC. Addition of 30 mol% cholesterol induces a significant, 2–4°C, increase in T_m. Interestingly, T_m for unfolding of rhodopsin reconstituted into 1:1 mixture of di22:6-PC/16:0,18:1-PC is intermediate, relative to the T_m in pure di22:6-PC and 16:0,18:1-PC proteoliposomes with, and without cholesterol.

Fluorescence resonance energy transfer from lipid-specific probes to rhodopsin

To explore the possibility that rhodopsin has an affinity for certain types of lipids, which is driven by acyl chain unsaturation, we studied FRET in systems containing lipid fluorescent probes labeled with Py at the headgroup: di22:6-, di16:0-, and 16:0,22:6-PE-Py (Fig. 1). As shown on Fig. 3, rhodopsin is an efficient acceptor of Py fluorescence due to a strong spectral overlap between Py emission and rhodopsin absorption (Fig. 3 *B*). Because of the nature of their acyl chains, Py-labeled lipids are expected to behave in a manner similar to their parent di22:6-, di16:0-, and 16:0,22:6-PC lipids.

We examined the efficiency of Py–rhodopsin FRET in liposomes composed of a mixture of di22:6-PC, di16:0-PC, and cholesterol at two different molar proportions: 7:3:3 and 3:7:3. In each case, two independent sets of samples containing 1 mol% of either di22:6-PE-Py or di16:0-PE-Py were prepared. The rhodopsin concentration in the lipid membrane ranged from 0 (control sample) to 1.2 mol%. The steady-state fluorescence intensity readings were taken at two temperatures: 50°C, which is well above the di16:0-PC phase transition (41.5°C), and at 10°C, when part of di16:0-PC is expected be in the gel-state (A. Polozova and B. J. Litman, in preparation). The efficiency of Py–rhodopsin energy transfer, in dark-adapted proteoliposomes containing 70 mol% (of total phospholipid) di22:6-PC, was the same for both di22:6- and di16:0-PE-Py probes and independent of temperature (Fig. 4, *A* and *B*). In contrast to that, an increase of di16:0-PC content up to 70 mol% (of total phospholipid) at the expense of di22:6-PC results in significant change in energy transfer pattern. The efficiency of FRET becomes considerably higher for di22:6-PC probe, indicating sequestering of polyunsaturated lipids and rhodopsin into the same domains (Fig. 5 *A*). Although this difference is detectable at both temperatures studied, it becomes more pronounced at 10°C, when part of di16:0-PC is expected to be in gel phase (Fig. 5 *B*). In samples exposed to light, FRET efficiency for both di22:6- and di16:0-PE-Py probes increases concomitantly, due to a better spectral overlap of Py emission with bleached rhodopsin absorption (Fig. 3 *B*). However, change of the rhodopsin conformation induced by bleaching does not affect the overall pattern of FRET: the FRET efficiency is identical for both probes in proteoliposomes containing 70 mol% of di22:6-PC (Fig. 4, *C* and *D*), and

TABLE 1 Effect of lipid composition on rhodopsin unfolding parameters

Lipid Composition	Cholesterol (mol%)	T_m (°C)	Calorimetric enthalpy (kcal/K*mol)	Van't Hoff Enthalpy (kcal/K*mol)	$\Delta H_{cal}/\Delta H_{vH}$
di22:6PC	0	68.7 ± 0.11	163 ± 19	160 ± 13	1.02
	30	70.6 ± 0.46	154 ± 14	185 ± 13	0.83
16:0,22:6PC	0	69.9 ± 0.26	157 ± 33	154 ± 17	1.02
	30	72.8 ± 0.71	153 ± 9	160 ± 6	0.96
16:0,18:1PC	0	70.6 ± 0.78	176 ± 4	173 ± 11	1.01
	30	74.4 ± 0.85	187 ± 32	196 ± 15	0.95
di22:6PC/16:0,18:1PC(1:1)	0	69.1	144	150	1.13
	30	72.8	187	176	0.98
Disk membranes		73.8 ± 0.92	220 ± 11	250 ± 1	0.58

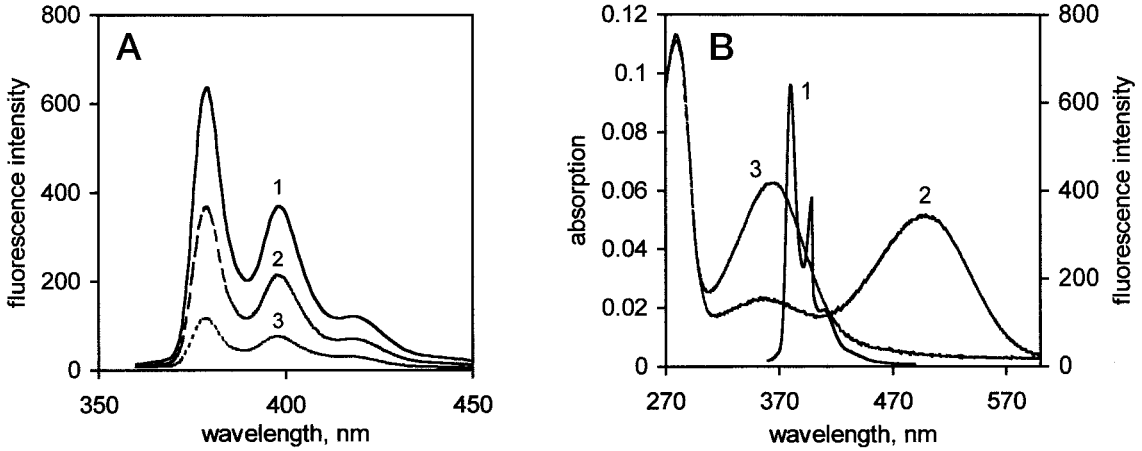

FIGURE 3 (*A*) Py emission intensity in the presence of different amounts of rhodopsin reconstituted in di22:6-PC/di16:0-PC/cholesterol (7:3:3) liposomes: *curve 1*, 0 mol%; *curve 2*, 0.2 mol%; *curve 3*, 1 mol%. Concentration of di22:6-PE-Py probe in the bilayer was 1 mol%. (*B*) Overlap of PE-Py emission and absorption spectra of rhodopsin reconstituted in di22:6-PC liposomes: *curve 1*, Py emission; *curve 2*, absorption of dark-adapted rhodopsin; *curve 3*, absorption of bleached rhodopsin.

the magnitude of the differences in samples containing 30 mol% of this lipid remains the same, compared to dark-adapted samples (Fig. 5, *C* and *D*).

Comparison between di22:6- and mixed-chain 16:0,22:6-PE-Py in proteoliposomes containing di22:6-PC; 16:0,22:6-PC, and cholesterol in 3:7:3 molar proportion did not reveal

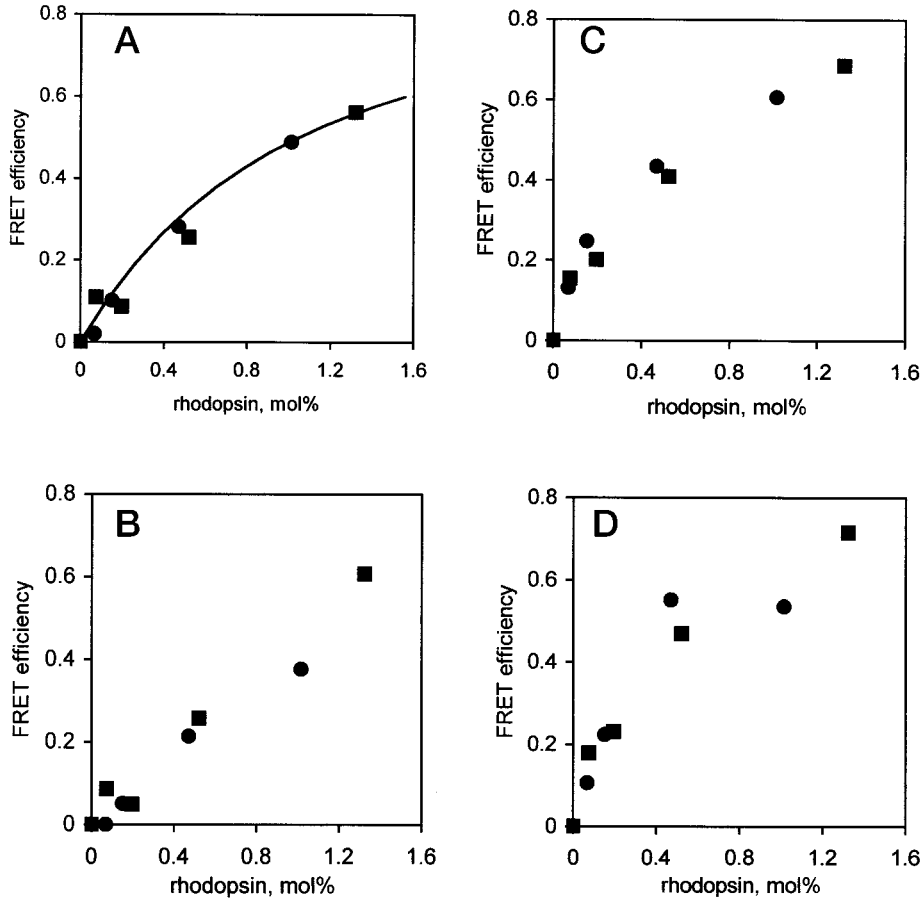

FIGURE 4 Py–rhodopsin FRET efficiency for (*A*, *B*) dark-adapted and (*C*, *D*) bleached di22:6-PC/di16:0-PC/cholesterol (7:3:3) proteoliposomes containing: ■, di22:6-PE-Py; ●, di16:0-PE-Py probes at (*A*, *C*) 50°C and (*B*, *D*) 10°C. *Solid curve*: theoretically calculated FRET efficiency, using distance of closest approach $\alpha = 1.8$ nm, and Förster radius $R_0 = 3.4$ nm (Appendix 2).

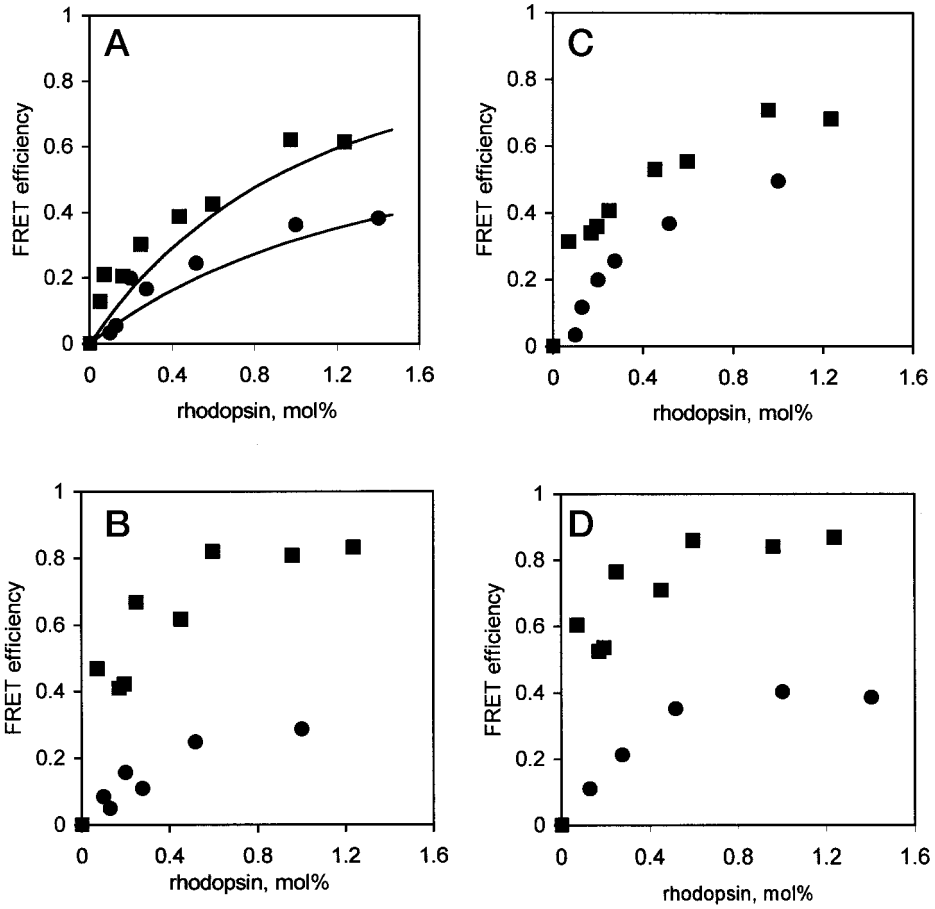

FIGURE 5 Py–rhodopsin FRET efficiency for (*A*, *B*) dark-adapted and (*C*, *D*) bleached di22:6-PC/di16:0-PC/cholesterol (3:7:3) proteoliposomes containing: ■, di22:6-PE-Py; ●, di16:0-PE-Py probes at (*A*, *C*) 50°C and (*B*, *D*) 10°C. *Solid curves:* theoretically calculated FRET efficiency for cluster model (Appendix 3). Parameters used in calculations: distance of closest approach α = 1.8 nm, Förster radius R_0 = 3.5 nm, cluster affinity coefficient for di22:6 lipid $\gamma = 3$.

any significant difference in efficiency of Py–rhodopsin FRET for the two probes (Fig. 6). Therefore, replacement of di16:0-PC by mixed-chain lipid 16:0,22:6-PC abolishes clustering of di22:6 lipids around the rhodopsin, at least within our detection limits.

To elucidate the role of cholesterol on the pattern of rhodopsin–lipid interactions, we prepared sets of samples containing 70 mol% di16:0-PC, 30 mol% di22:6-PC, and no cholesterol. In contrast to the previous observations (Fig. 5), there is no difference in energy transfer efficiency from either di22:6-PE-Py, or di16:0-PE-Py probes to rhodopsin at 50°C, when all lipid is in liquid-crystalline state (Fig. 7 *A*). But at 10°C, which is well below main phase transition of di16:0-PC (41.5°C), the significantly higher energy transfer efficiency was observed for di22:6-PE-Py probe (Fig. 7 *B*). Unlike in the case of samples containing cholesterol (Fig. 5, *B* and *D*), this difference disappeared after the rhodopsin was bleached (Fig. 7 *D*). Therefore, the presence of choles-

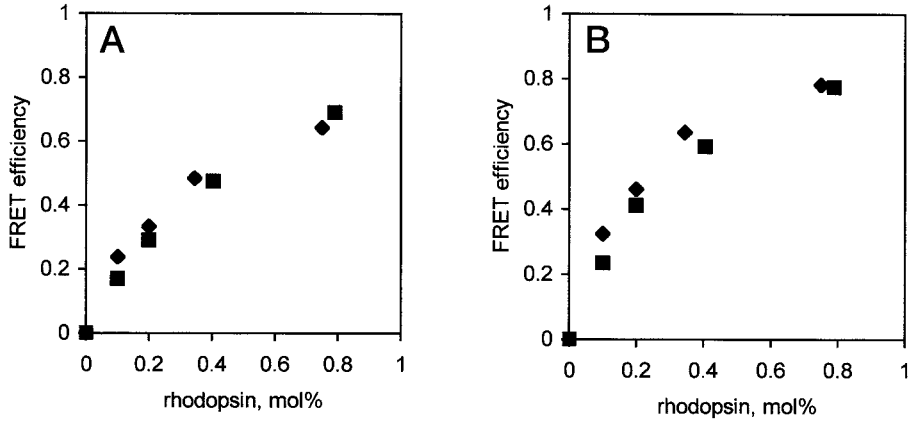

FIGURE 6 Py–rhodopsin RET efficiency for (*A*) dark-adapted and (*B*) bleached di22:6-PC/16:0,22:6-PC/cholesterol (3:7:3) proteoliposomes containing: ■, di22:6-PE-Py and ♦, 16:0,22:6-PE-Py probes at 25°C.

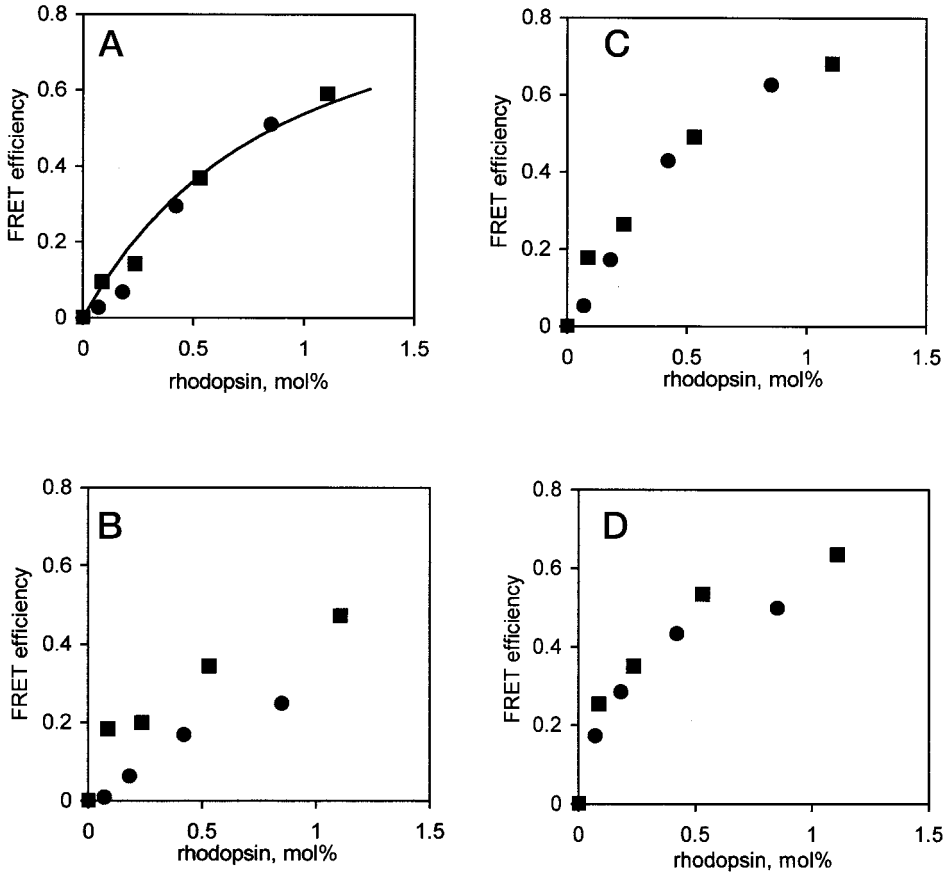

FIGURE 7 Py–rhodopsin RET efficiency for (*A*, *B*) dark-adapted and (*C*, and *D*) bleached di22:6-PC/di16:0-PC (3:7) proteoliposomes containing: ■, di22:6-PE-Py; ●, di16:0-PE-Py probes at (*A*, *C*) 50°C and (*B*, *D*) 10°C. *Solid curve:* theoretical calculation of FRET efficiency using distance of closest approach $\alpha = 2.2$ nm and Förster radius $R_0 = 3.5$ nm (Appendix 2).

terol is important for maintaining the pattern of rhodopsin–lipid interactions in the liquid-crystalline state.

DISCUSSION

Stability of rhodopsin in native and reconstituted membranes

Effects of the lipid environment on the structure of membrane proteins manifest themselves in the parameters of thermal denaturation curves. The mid-transition point, T_m, is a direct measure of protein stability, whereas a comparison of the calorimetric (ΔH_{cal}) and van't Hoff (ΔH_{vH}) enthalpies provides insight into the details of the unfolding process and underlying features of intra- and interprotein organization in the membrane. Deviation of $\Delta H_{cal}/\Delta H_{vH}$ from unity to higher values usually implies that the unfolding transition involves several steps, whereas ratios less than one generally indicate that protein–protein interactions are present, which must be overcome during denaturation (Sturtevant, 1987). In most reconstituted samples of rhodopsin, the $\Delta H_{cal}/\Delta H_{vH}$ ratio is very close to one, pointing to a simple two-state unfolding process (Table 1). The only exception is a sample of proteoliposomes containing di22:6-PC and 30 mol% cholesterol. In this case, the $\Delta H_{cal}/\Delta H_{vH}$ ratio is only 0.83, and it is even lower for native disk membranes (0.58). Such low $\Delta H_{cal}/\Delta H_{vH}$ values generally indicate cooperativity between rhodopsin molecules as they unfold. Although the extensive direct rhodopsin–rhodopsin aggregation is unlikely (Cone, 1972; Kusumi and Hyde, 1982), the lipids can mediate a certain extent of transient association of rhodopsin or lipid–rhodopsin complexes. Therefore, calorimetric data on unfolding of rhodopsin in bilayers containing di22:6-PC and cholesterol point to the existence of additional protein coupling in such membranes. The known tendency of cholesterol to separate out of di22:6 lipids and interact preferentially with saturated lipids (Huster et al., 1998; Brzustowicz et al., 1999) may aid in formation of domains enriched with di22:6-PC and rhodopsin. This would create areas with higher protein surface density and result in additional coupling at thermal denaturation.

Clustering of lipids around the rhodopsin

Fluorescence energy transfer in the liposome membrane between the Py fluorophore attached to the lipid headgroup and retinal located inside the membrane protein rhodopsin fits well into the model of random planar array of donors and acceptors developed by Fung and Stryer (1978). The use of this model in application to our system is valid if: 1) there is no energy transfer between donors, and 2) the

distance between donors and acceptors does not change significantly during the donor-excited state lifetime. The first condition was assured by choosing appropriate Py probe concentration (see Experimental Procedures), whereas the second condition was verified by evaluating the PE-Py diffusion coefficient (Appendix 1). From diffusion coefficients and lifetime data of Py probes (Table 2), the mean square displacement during the lifetime of the excited state was estimated as 10–20 Å^2, using relationship $\langle r\rangle^2 = 4 \times D \times \tau$ (D is diffusion coefficient and τ is the excited state lifetime). Such probe displacement is much less than the area occupied by both types of single lipids (62 and 76 Å^2). Therefore, we can assume that condition (2) appears to be valid and the observed transfer efficiency is the static average over the ensemble of all donor–acceptor pairs.

According to the theory, the energy transfer efficiency between donors and acceptors randomly arranged in the membrane, is a function of the characteristic Förster radius R_0 (distance between donor and acceptor at which the transfer efficiency is 50%), the distance of the closest approach of donor and acceptor α, and the surface density of acceptors σ (Fung and Stryer, 1978). Förster R_0 radius of a pyrene–rhodopsin donor–acceptor pair was estimated to be in the range 25–37 Å (for details see Appendix 2). It is known that the retinal is located in the middle of the rhodopsin (Liebman, 1962; Thomas and Stryer, 1982; Han and Smith, 1995). Noting that the planar dimensions of rhodopsin are 28 × 39 Å (Unger et al., 1997), the thickness of bilayer composed of lipids used in this study is about 38 Å (K. Gawrisch and B. W. Koenig, unpublished results), and the pyrene molecular radius is about 3.6 Å (Edward, 1970), we estimate that α, the distance of donor–acceptor closest approach, is in the range of 18–31 Å, depending on the location of fluorophore. The best fit for experimental data on FRET for di22:6-PC–di16:0-PC–cholesterol (7:3:3) liposomes was obtained with a combination of $R_0 = 34$ Å and $\alpha = 18$ Å (Fig. 4 *A*).

The fluorescence energy transfer in proteoliposomes composed of di22:6-PC–di16:0-PC–cholesterol at (7:3:3) proportion, or di22:6-PC–16:0,22:6-PC–cholesterol at (3:7:3) proportion is well described by random distribution model for all examined lipid-specific probes. However, in the case of proteoliposomes containing more di16:0-PC at the expense of di22:6-PC (di22:6-PC–di16:0-PC–cholesterol at (3:7:3) proportion), there is a clear deviation from the random distribution of donor–acceptor pairs, because the energy transfer efficiency is considerably higher for the di22:6-specific probe, compared to the di16:0-specific one. To account for this discrepancy, we developed a cluster model, assuming the existence of areas enriched with di22:6-PC lipid around each rhodopsin molecule (Fig. 8, Appendix 3). The overall energy transfer efficiency is then represented by a combination of two contributions: $E = E_c + E_b$, where E_c and E_b are the transfer contributions of donors in the clusters and in the rest of the bulk bilayer. In this case, the FRET efficiency is a function of cluster size, represented by radius R_c (for simplicity the clusters are assumed to be of round shape), and γ, the affinity of di22:6 lipid to the clusters, in addition to R_0, σ and α described above. In the theoretical model, the affinity coefficient γ represents the ratio of two phospholipid types in the cluster: $\gamma_{22:6} = N^c_{22:6}/N^c_{16:0}$, $\gamma_{16:0} = N^c_{16:0}/N^c_{22:6}$, where $N^c_{22:6}$ and $N^c_{16:0}$ are numbers of di22:6-PC and di16:0-PC lipids in each cluster formed around rhodopsin. Fitting of experimental data for both di22:6- and di16:0-PE-Py probes was performed in a coupled manner. For the fitting of data corresponding to di16:0-specific probe, the affinity coefficient was set as the reciprocal of the one corresponding to di22:6-specific probe: $\gamma_{16:0} = 1/\gamma_{22:6}$.

The best fit of experimental data was achieved with $R_c = 35$ Å and $\gamma = 3$. The significance of this finding is that it provides direct information about the characteristic range of the rhodopsin–lipid interactions. Given the evaluated cluster size, the range of the interactions exceeds two lipid layers adjacent to the protein. The affinity coefficient γ has a level of uncertainty associated with it, because it involves the degree of possible deviation of the di22:6- or di16:0-PE-Py probe distribution from the bulk lipid composition. The theoretical curve for di16:0-PE-Py probe is slightly below the corresponding experimental points (Fig. 5 *A*). Such discrepancy can be due to deviation of probe distribution from the distribution of parent di16:0-PC lipid. Due to bulky

TABLE 2 Properties of lipid-specific Py probes

Probe Type	Temperature (°C)	Monomer Lifetime* (ns)	Excimer/Monomer# (I′/I)	Excimer Lifetime§ (ns)	Diffusion Coefficient¶ (cm^2/s)
di22:6-PE-Py	50	18.8 ± 0.3	0.2	30.3 ± 0.08	2.6×10^{-8}
	10	20.7 ± 0.4			
di16:0-PE-Py	50	21.6 ± 0.3	0.14	43.8 ± 0.11	1.4×10^{-8}
	10	26.2 ± 0.5			
16:0,22:6-PE-Py	25	24.6 ± 0.3	0.16	36 ± 2	

*§Monomer and excimer emission decays were almost monoexponential, with less than 4% contribution from the second process.

#I′ was measured at 490 nm, I was measured at 380 nm; the membrane probe concentrations (in number of molecules per Å^2) were: di22:6-PE-Py, 1.27×10^{-3} Å^{-2}; di16:0-PE-Py, 1.13×10^{-3} Å^{-2}; 16:0,22:6-PE-Py, 1.54×10^{-3} Å^{-2}.

¶Calculated using equation in Appendix 1.

pyrene fluorhophore attached to the lipid headgroup, this probe may slightly favor the polyunsaturated lipid environment, compared to the parent lipid. In this case, the measured values of FRET efficiency should be higher than calculated ones, because the theoretical model does not take into account such deviation in distribution.

Using the evaluated proportion of two lipid types in the clusters, one can explain the observed FRET difference between proteoliposomes containing 70 mol% (of total phospholipid) of di22:6-PC and the ones containing only 30 mol% of this lipid. The value of the affinity coefficient γ is related to the proportion of di22:6-PC in the cluster. If the overall proportion of this lipid in the bilayer is close to the one in the cluster, then there will be no distinct difference between the cluster and bulk bilayer compositions. In the case of proteoliposomes containing 70 mol% of di22:6-PC and 30 mol% of di16:0-PC, the di22:6-PC/di16:0-PC ratio is 2.3, which is much closer to the calculated affinity coefficient value, $\gamma = 3$. In contrast to that, in the case of 30 mol% of di22:6-PC, this ratio is only 0.43. Thus, the di22:6-PC-enriched clusters in the 70 mol% di22:6-PC bilayer have a composition closely approximating the bulk bilayer and, therefore, are undetectable.

ROLE OF CHOLESTEROL

Comparison between sets of samples containing mixtures of di22:6-PC and di16:0-PC at 3:7 proportion (Figs. 5 and 7) clearly shows that the presence of cholesterol is a crucial factor inducing segregation of rhodopsin with polyunsaturated lipids when the bilayer is in liquid-crystalline state. The association of rhodopsin with di22:6 lipids at 50°C, revealed by the higher FRET efficiency for di22:6-PE-Py, was detected only in the presence of 30 mol% cholesterol. As cholesterol preferentially interacts with saturated di16:0-PC (Mitchell and Litman, 1998; Huster et al., 1998; Brzustowicz et al., 1999), it probably promotes the lateral separation of this lipid into the cholesterol-enriched domains, whereas rhodopsin partitions into areas enriched with di22:6-PC. At low temperature, the lateral separation is most likely driven by the transition of di16:0-PC into gel state. Under these conditions, rhodopsin retains the tendency to associate with polyunsaturated lipids. It is important to note that the rhodopsin itself is an essential factor defining membrane organization. In pure lipid bilayers of similar composition, no cluster formation was detected (A. Polozova and B. J. Litman, in preparation). Therefore, segregation of rhodopsin with di22:6-PC is based on their mutual affinity for each other, rather than on partitioning of this protein into existing clusters.

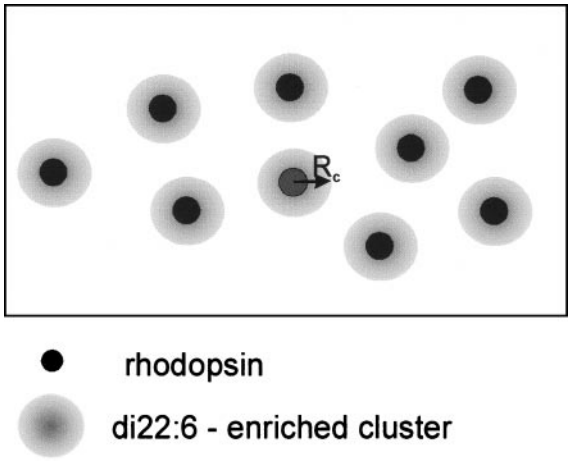

FIGURE 8 Cluster model of rhodopsin–lipid organization in the membrane.

Another important functional role of cholesterol is related to the preservation of protein integrity. Comparison of Figs. 5 *D* and 7 *D* shows that only in the presence of cholesterol does the overall pattern of energy FRET efficiency to both probes remain the same after the rhodopsin bleaching. The loss of discrimination of bleached rhodopsin between di22:6- and di16:0-PE-Py probes in the absence of cholesterol (Fig. 7 *D*), may indicate loss of the native protein conformation, followed by disruption of the overall membrane organizational pattern.

CONCLUSIONS

The lipid environment profoundly affects stability and intramembrane organization of rhodopsin. The higher level of lipid unsaturation results in lower rhodopsin stability, whereas cholesterol increases protein stability and promotes intramembrane protein–protein associations.

The remarkable ability of polyunsaturated lipids to associate with rhodopsin, even when the mixed bilayer is in liquid-crystalline phase, is directly coupled with the presence of the protein itself and the cholesterol. Preferential interaction of cholesterol with saturated acyl chains promotes membrane lateral separation onto domains enriched in di16:0-PC and cholesterol, and di22:6-PC and rhodopsin, respectively. Di22:6-PC-enriched domains are centered around each rhodopsin molecule and contain at least two layers of phospholipid adjacent to protein. Such clusters were detected only in mixtures of symmetrically substituted di22:6- and di16:0-PC lipids, and the level of enrichment in polyunsaturated lipid was estimated to be a factor of six.

These findings once again point to the importance of lipid–protein interactions in modulating the function of membrane proteins, and demonstrate that acyl chain unsaturation is an important factor facilitating structural organization of biological membranes.

APPENDIX 1: ESTIMATION OF DIFFUSION COEFFICIENTS OF PE-Py PROBES

Formation of excited pyrene dimers (excimers) in fluid membranes is a diffusion-controlled process. The extent of excimer formation of the flu-

orophore is directly related to the diffusion coefficient as given by

$$D_{\text{diff}} = \frac{I'}{kI} \cdot \frac{k_f}{k_f'} \cdot \frac{\lambda}{4 d_c \tau_0' c},$$

where I and I' are monomer and excimer intensities; k is a proportionality coefficient relating I/I' to quantum yields ratio; k_f and k_f' are radiation transition probabilities for monomer and excimer; λ is the length of one diffusional jump; d_c is the Van der Waals diameter; c is the concentration of the diffusing phospholipid probes measured in units of molecules per Å^2; and τ_0' is the excimer lifetime (Galla and Sackmann, 1974). The ratio k_f/k_f' is the intrinsic property of the fluorophore molecule, and, for Py, it is approximately 0.1 (Galla and Sackmann, 1974). The quantum yield-intensity proportionality coefficient for PE-Py probes was evaluated as $k = 0.5$. The diffusional jump length λ and Van der Waals diameter d_c were assumed to be equal to one lipid diameter, approximately 10 Å. The results of diffusion coefficients calculations are summarized in Table 2.

APPENDIX 2: CALCULATION OF FÖRSTER RADIUS R_0 AND FRET EFFICIENCY FOR PE-Py–RHODOPSIN DONOR/ACCEPTOR PAIR

According to the theory of fluorescence resonance energy transfer developed by Förster (1948), R_0, the distance between donor and acceptor at which the transfer efficiency is 50%, is given by

$$R_0^6 = (JK^2 Q_0 n^{-4}) \times (8.79 \times 10^{-28}\ \text{mol}),$$

where Q_0 is the quantum yield of donor in the absence of acceptor; n is the refractive index of the medium; and K^2 is the dipole–dipole orientational factor. J is the spectral overlap integral (in cm^6/mol), given by

$$J = \frac{\int F_D(\lambda)\varepsilon_A(\lambda)\lambda^4\, d\lambda}{\int F_D(\lambda)\, d\lambda},$$

where $F_D(\lambda)$ is the fluorescence intensity of the donor in the absence of acceptor at the wavelength λ, and $\epsilon_A(\lambda)$ is the molar absorption coefficient of the acceptor at λ.The overlap integral was estimated from PE-Py emission and rhodopsin adsorption spectra as 1.46×10^{-12} cm^6/mol, the quantum yield was evaluated as 0.98, and the refractive index was assumed to be 1.44. Minimum and maximum values of orientational factor were evaluated from depolarization factors of donor and acceptor according to (Dale et al., 1979)

$$\langle K^2\rangle_{\max} = 2/3(1 + \langle d_D\rangle + \langle d_A\rangle + 3\langle d_D\rangle\langle d_A\rangle)$$

$$\langle K^2\rangle_{\min} = 2/3[1 - (\langle d_D\rangle + \langle d_A\rangle)/2],$$

where $\langle d_D\rangle$ and $\langle d_A\rangle$ are donor and acceptor depolarization factors, subsequently. The depolarization factor for the acceptor can be calculated using relationship $\langle d_D\rangle = (r_\infty/r_o)^{1/2}$, where r_o and r_∞ are the fundamental and limiting and anisotropies. The measured values for PE-Py probes are: $r_o = 0.33$ and $r_\infty = 0.003$ (see Experimental section for details). Therefore, $\langle d_D\rangle$ is evaluated as 0.095, whereas $\langle d_A\rangle = 1$ can be assumed for rhodopsin, because its rotation correlation time does not exceed 10^{-6} s (Cone, 1972; Kusumi and Hyde, 1982; Ryba and Marsh, 1992). Therefore, the overall orientation should not change significantly during the donor lifetime (~20 ns). Using these values, the range of possible orientational factors was evaluated as 0.30–1.6, which resulted in the following estimate of Förster radius: $27 < R_0 < 37$ Å.

According to the theory of FRET for donors and acceptor in the random array in plane of the membrane, the efficiency of energy transfer is given by the following set of equations:

$$E = 1 - (t/\tau)\int_0^\infty F(t)/F(0)\ \mathrm{d}t, \qquad \text{(A1)}$$

$$F(t) = F(0)\exp(-t/\tau)\exp(-\sigma \cdot S(t)), \qquad \text{(A2)}$$

$$S(t) = \int_\alpha^\infty \{1 - \exp[-(t/\tau)(R_0/r)^6]\} 2\pi r\ \mathrm{d}r, \qquad \text{(A3)}$$

where E is the transfer efficiency; $F(t)$ is the fluorescence intensity of donor at time t following a very short light flash; $S(t)$ is the energy transfer term; τ is the lifetime of donor in the absence of acceptor; and σ is the surface density of acceptors (Fung and Stryer, 1978). The numerical integration of these equations was performed to fit the experimental data on energy transfer presented on Fig. 4, *A* and *B*. The acceptor surface density used in the calculations was corrected for the difference in protein and lipid size:

$$\sigma = \frac{N_r \cdot A_r}{N_r \cdot A_r + N_l \cdot A_l} \cdot \frac{A_{\text{ret}}}{A_r} = \frac{1}{1 + (A_l/A_r)\cdot(1/p)} \cdot \frac{A_{\text{ret}}}{A_r}, \qquad \text{(A4)}$$

where N_r, N_l, A_r, and A_l are the number and areas of rhodopsin molecules and lipids in each given sample; and p is the rhodopsin-to-lipid molar ratio. A_l was calculated as the average area per lipid, taking into account proportions of different lipids and cholesterol in each given liposome composition. The following values were used in calculations: $A_r = 1307$ Å^2 (Krebs et al., 1998), $A_{\text{ret}} = 210$ Å^2 (Liu and Mirzadegan, 1988), $A_{\text{di22:6PC}} = 76$ Å^2 (K. Gawrisch and B.W. Koenig, unpublished results), $A_{\text{di16:0PC}} = 62$ Å^2 (Petrache et al., 1999), $A_{16:0,22:6\text{PC}} = 69$ Å^2 (Koenig et al., 1997), and $A_{\text{cholest}} = 32$ Å^2 (Engelman and Rothman, 1972). To take into account the condensing effect of cholesterol, we assumed that it affects only di16:0-PC lipid (Mitchell and Litman, 1998; Huster et al., 1998). The molar proportion of cholesterol was recalculated with respect to the fraction of di16:0PC in each bilayer composition. The average condensed cross-sectional area per di16:0-PC at 50°C was assumed to be about 40 Å (Ipsen et al., 1990). To achieve the best fit of experimental data, two parameters were varied: the Förster radius R_0, restricted by the range $27\ \text{Å} < R_0 < 37$ Å, and the distance of the closest approach α, restricted by the range 18–30 Å. The range of possible α values was deduced from geometrical considerations of donor and acceptor molecular dimensions and their possible location: retinal was assumed to be in the middle of the rhodopsin (Liebman, 1962; Thomas and Stryer, 1982; Han and Smith, 1995), and Py fluorophore was assumed to be near the bilayer interface, with possible penetration into the hydrophobic core. The following values were used in calculations: 28 × 39 Å as planar dimensions of rhodopsin (Unger et al., 1997), 38 Å as thickness of bilayer composed of lipids used in this study (K. Gawrisch and B.W. Koenig, unpublished results), and 3.6 Å as pyrene molecular radius (Edward, 1970).

The best fit was obtained with $R_0 = 34$ Å and $\alpha = 18$ Å for FRET data of di22:6-PC/di16:0-PC/cholesterol (7:3:3) mixed system, $R_0 = 35$ Å and $\alpha = 22$ Å for di22:6-PC/di16:0-PC (3:7) system.

APPENDIX 3: CLUSTER MODEL OF PROTEIN–LIPID ORGANIZATION

To describe the organization of mixed bilayer containing two lipids with different affinity for membrane protein, we propose a simplified cluster model. One can assume that there is a lipid cluster formed around each rhodopsin, and the composition of this cluster is different from the bulk bilayer composition. The cluster is characterized by its size and partition

coefficient of lipid between the cluster and the rest of the bilayer. For simplicity, we assume that: 1) the cluster is of a round shape, therefore its size can be characterized by radius R_c; 2) the lipid distribution inside the cluster and in the rest of bilayer is homogeneous; and 3) the lipid composition in the cluster is described by coefficient $\gamma_{22:6} = N_{22:6}/N_{16:0}$, reflecting the affinity of lipid to the cluster ($N_{22:6}$ and $N_{16:0}$ are the numbers of lipid in the cluster, containing 22:6 and 16:0 hydrocarbon chains).

The emission kinetics of the fluorescence donor in such system can be described as

$$F(t) = F(0)\exp(-t/\tau)[f_c \exp(-\sigma_c S_c(t)) + (1 - f_c)\exp(-\sigma_b S_b(t))], \quad \text{(A5)}$$

where f_c is a fraction of donors in the clusters; σ_c, σ_b are acceptor surface densities in clusters and in bulk bilayer; and $S_c(t)$, $S_b(t)$ are transfer terms for clusters and bulk bilayer. The fraction of donors in the clusters, taking into account partition coefficient γ, is given by

$$f_c = \frac{(\pi R_c^2 - A_r)\cdot N_r}{N_r A_r + N_l A_l} \cdot \frac{1 + N_{di16:0}/N_{di22:6}}{1 + 1/\gamma} = \frac{\pi R_c^2 - A_r}{A_r + A_l/p} \cdot \frac{1 + N_{di16:0}/N_{di22:6}}{1 + 1/\gamma}, \quad \text{(A6)}$$

where N_r, N_l, A_r, A_l, and p are the same as described above (Appendix 2). (A_l used in calculations was a weighted average area per lipid in the mixed bilayer composed of di22:6-PC, di16:0-PC, and cholesterol. There is a slight difference in average area per lipid in clusters and in bulk bilayer due to the difference in composition. If this difference is accounted for in Eq. A6, it results in very minor changes in final calculated FRET efficiency. Therefore, it was omitted for simplicity. Acceptor surface density in the clusters is independent on the overall protein/lipid ratio and is given by

$$\sigma_c = \frac{A_{ret}}{\pi R_c^2}, \quad \text{(A7)}$$

whereas σ_b is equivalent to σ given by Eq. A4.

The transfer terms for clusters and bulk bilayer can be expressed as

$$S_c(t) = \int_{\alpha}^{R_c} \{1 - \exp[-(t/\tau)(R_0/r)^6]\} 2\pi r \, dr, \quad \text{(A8)}$$

$$S_b(t) = \int_{R_c}^{\infty} \{1 - \exp[-(t/\tau)(R_0/r)^6]\} 2\pi r \, dr. \quad \text{(A9)}$$

Substitution of Eqs. A4–A9 into A1 and rearrangement of terms gives a simple expression

$$E = E_c + E_b, \quad \text{(A10)}$$

where

$$E_c = f_c \cdot \left[1 - (1/\tau)\int_0^{\infty} \exp(-t/\tau)\exp(-\sigma_c S_c(t))\, dt\right], \quad \text{(A11)}$$

$$E_b = (1 - f_c)\cdot \left[1 - (1/\tau)\int_0^{\infty} \exp(-t/\tau)\exp(-\sigma S_b(t))\, dt\right]. \quad \text{(A12)}$$

Eq. A10, describing the overall FRET efficiency is a function of R_c and γ, in addition to R_0 and α. The fit of experimental data, presented on Fig. 5 *A*, was performed only by varying R_c and γ, and assuming that the affinity coefficient of di22:6-PE-Py probe is related to one of di16:0-PE-Py probe because $\gamma_{16:0} = 1/\gamma_{22:6}$. The fit of Eq. 10 was performed simultaneously for di22:6- and di16:0-PE-Py probes. The best fit was achieved at the following set of parameters: $R_0 = 3.5$ nm, $\alpha = 1.8$ nm, $R_c = 3.5$ nm, and $\gamma = 3$.

The authors are grateful to Dr. D. C. Mitchell for measurements of lifetimes of Py-PE probes and for stimulating discussion. We also thank Dr. S.-L. Niu for help in determining the optimal conditions for the dialysis procedure.

REFERENCES

Anderson, R. E., D. J. Landis, and P. A. Dudley. 1979. Essential fatty acid deficiency and renewal of rod outer segments in the albino rat. *Inv. Ophtal.* 15:232–236.

Brown, D. A., and E. London. 1998. Structure and origin of ordered lipid domains in biological membranes. *J. Membrane Biol.* 164:103–114.

Brzustowicz, M. R., W. Stillwell, and S. R. Wassall. 1999. Molecular organization of cholesterol in polyunsaturated phospholipid membranes: a solid state ^{2}H NMR investigation. *FEBS Lett.* 451:197–202.

Christensen, H., N. J. Garton, R. Horobin, D. Minnikin, and M. R. Barer. 1999. Lipid domains of mycobacteria studied with fluorescent molecular probes. *Molec. Microbiol.* 31:1561–1572.

Cone, R. A. 1972. Rotational diffusion of rhodopsin in the visual receptor membrane. *Nat. New Biol.* 236:39–43.

Dale, R. E., J. Eisinger, and W. E. Blumberg. 1979. The orientational freedom of molecular probes. The orientation factor in intermolecular energy transfer. *Biophys. J.* 26:161–194.

Dumas, F., M. M. Sperotto, M.-C. Lebrun, J.-F. Tocanne, and O. G. Mouritsen. 1997. Molecular sorting of lipids by bacteriorhodopsin in dilauroylphosphatidylcholine/distearoylphosphatidylcholine lipid bilayers. *Biophys. J.* 73:1940–1953.

Edward, J. T. 1970. Molecular volumes and the Stokes–Einstein equation. *J. Chem. Educ.* 47:261–270.

Engelman, D. M., and J. E. Rothman. 1972. The planar organization of lecithin–cholesterol bilayers. *J. Biol. Chem.* 247:3694–3697.

Ferretti, A., A. Knijn, E. Iorio, S. Pulciani, M. Giambenedetti, A. Molinari, S. Meschini, S. Stringaro, A. Calcabrini, I. Freitas, R. Strom, G. Arancia, and F. Podo. 1999. Biophysical and structural characterization of H-1-NMR-detectable mobile lipid domains in NIH-3T3 fibroblasts. *Biochim. Biophys. Acta.* 1438:329–348.

Förster, T. 1948. Intermolecular energy migration and fluorescence. *Ann. Physik. (Leipzig)* 2:55–75.

Fredrichson, T., and T. V. Kurzchalia. 1998. Microdomains of GPI-anchored proteins in living cells revealed by crosslinking. *Nature.* 394: 802–805.

Fung, B. K.-K., and L. Stryer. 1978. Surface density determination in membranes by fluorescence energy transfer. *Biochemistry*. 17: 5241–5248.

Galla, H.-J., and E. Sackmann. 1974. Lateral diffusion in the hydrophobic region of membranes: use of pyrene excimer as optical probes. *Biochim. Biophys. Acta.* 339:103–115.

Han, M., and S. O. Smith. 1995. NMR constraints on the location of the retinal chromophore in rhodopsin and bathorhodopsin. *Biochemistry*. 34:1425–1432.

Harder, T., P. Scheiffele, P. Verkade, and K. Simons. 1998. Lipid domain structure of the plasma membrane revealed by patching of membrane components. *J. Cell Biol.* 141:929–942.

Hooper, N. M. 1999. Detergent-insoluble glycosphingolipid/cholesterol-rich domains, lipid rafts and caveolae. *Mol. Membr. Biol.* 16:145–156.

Huster, D., K. Arnald, and K. Gawrisch. 1998. Influence of docosahexaenoic acid and cholesterol on lateral lipid organization in phospholipid mixtures. *Biochemistry*. 37:17299–17308.

Hwang, J., L. A. Gheber, L. Margolis, and M. Edidin. 1998. Domains in cell plasma membranes investigated by near-field scanning optical microscopy. *Biophys. J.* 74:2184–2190.

Ipsen, J. H., O. G. Mouritsen, and M. Bloom. 1990. Relationship between lipid membrane area, hydrophobic thickness, and acyl-chain orientational order. *Biophys. J.* 57:405–412.

Jackson, M. L., and B. J. Litman. 1982. Rhodopsin-phospholipid reconstitution by dialysis removal of octyl glucoside. *Biochemistry*. 21: 5601–5608.

Jackson, M. L., and B. J. Litman. 1985. Rhodopsin-egg phosphatidylcholine reconstitution by an octyl glucoside dilution procedure. *Biochim. Biophys. Acta.* 812:369–376.

Keller, S. L., W. H. Pitcher, III, W. H. Huestis, and H. M. McConnell. 1998. Red blood cell lipids form immiscible liquids. *Phys. Rev. Lett.* 81:5019–5022.

Khan, S. M. A., W. Bolen, P. A. Hargrave, M. M. Santoro, and J. H. McDowell. 1991. Differential scanning calorimetry of bovine rhodopsin in rod-outer-segment disk membranes. *Eur. J. Biochem.* 200:53–59.

Kinnunen, P. K. J., A. Koiv, J. Y. A. Lehtonen, M. Rytomaa, and P. Mustonen. 1994. Lipid dynamics and peripheral interactions of proteins with membrane surfaces. *Chem. Phys. Lip.* 73:181–207.

Koenig, B. W., H. H. Strey, and K. Gawrisch. 1997. Membrane lateral compressibility determined by NMR and X-ray diffraction: effect of acyl chain polyunsaturation. *Biophys. J.* 73:1954–1966.

Krebs, A., K. Villa, P. C. Edwards, and G. F. X. Schertler. 1998. Characterization of an improved two-dimensional $p22_12_1$ crystal from bovine rhodopsin. *J. Mol. Biol.* 282:991–1003.

Kusumi, A., and J. S. Hyde. 1982. Spin-label saturation-transfer electron spin resonance detection of transient association of rhodopsin in reconstituted membranes. *Biochemistry*. 21:5978–5983.

Liebman, P. A. 1962. In situ microspectrophotometric studies on the pigments of single retinal rods. *Biophys. J.* 2:161–178.

Litman, B. J. 1982. Purification of rhodopsin by concanavalin A affinity chromatography. *Methods Enzymol.* 81:150–153.

Litman, B. J., and D. C. Mitchell. 1996. A role of phospholipid polyunsaturation in modulating membrane protein function. *Lipids*. 31: S193.–S197.

Liu, R. S. H., and T. Mirzadegan. 1988. The shape of a three-dimensional binding site of rhodopsin based on molecular modeling analysis of isomeric and other visual pigment analogues. Bioorganic studies of visual pigments. *J. Am. Chem. Soc.* 110:8617–8623.

Marsh, D. 1995. Lipid–protein interactions and heterogeneous lipid distribution in membranes. *Molec. Membr. Biol.* 12:59–64.

Masserini, M., P. Palestini, and M. Pitto. 1999. Glycolipid-enriched caveolae and caveolae-like domains in the nervous system. *J. Neurochem.* 73:1–11.

Miljanich, G. P., M. F. Brown, S. Mabrey-Gaud, E. Dratz, and J. M. Sturtevant. 1985. Thermotropic behavior of retinal rod membranes and dispersions of extracted phospholipids. *J. Membr. Biol.* 85:79–86.

Miljanich, G. P., L. A. Sklar, D. L. White, and E. A. Dratz. 1979. Disaturated and dipolyunsaturated phospholipids in the bovine retinal rod outer segment disk membrane. *Biochim. Biophys. Acta*. 552: 294–306.

Mitchell, D. C., and B. J. Litman. 1998. Effect of cholesterol on molecular order and dynamics in highly polyunsaturated phospholipid bilayers. *Biophys. J.* 75:896–908.

Mitchell, D. C., M. Straume, and B. J. Litman. 1992. Role of *sn*-1-saturated, *sn*-2-polyunsaturated phospholipids in control of membrane receptor conformational equilibrium: effects of cholesterol and acyl chain composition on the metarhodopsin I–metarhodopsin II equilibrium. *Biochemistry*. 31:662–670.

Mitchell, D. C., K. Gawrisch, B. J. Litman, and N. Salem, Jr. 1998. Why is docosahexaenoic acid essential for nervous system function? *Biochem. Soc. Trans.* 26:365–370.

Mouritsen, O. G. 1998. Self-assembly and organization of lipid–protein membranes. *Curr. Opinion Coll. Int. Sci.* 3:78–87.

Petrache, H. I., T. Kechuan, and J. F. Nagle. 1999. Analysis of simulated NMR order parameters for lipid bilayer structure determination. *Biophys. J.* 76:2479–2487.

Ryba, N. J. P., and D. Marsh. 1992. Protein rotational diffusion and lipid protein interactions in recombinants of bovine rhodopsin with saturated diacylphosphatidylcholines of different chain length studied by conventional and saturation-transfer electron-spin-resonance. *Biochemistry*. 31: 7511–7518.

Salem, N., Jr.1989. Omega-3 fatty acids: molecular and biochemical aspects. *In* New Protective Role for Selected Nutrients. G. A. Spiller, and J. Scala, editors. Alan R. Liss Inc., New York.108–228.

Shnyrov, V. L., and A. L. Berman. 1988. Calorimetric study of thermal denaturation of vertebrate visual pigments. *Biomed. Biochim. Acta.* 47:355–362.

Singer, S. J., and G. L. Nicholson. 1972. The fluid mosaic model of the structure of cell membranes. *Science.* 75:720–731.

Spiro, R. G. 1966. Analysis of sugars, found in glycoproteins. *Methods Enzymol.* 8:3–26.

Stone, W. L., C. C. Farnsworth, and E. A. Dratz. 1979. A reinvestigation of the fatty acid content of bovine, rat and frog retinal rod outer segments. *Exp. Eye Res.* 28:387–397.

Sturtevant, J. M. 1987. Biochemical applications of differential scanning calorimetry. *Ann. Rev. Phys. Chem.* 38:463–488.

Thomas, D. D., and L. Stryer. 1982. Transverse location of the retinal chromophore of rhodopsin in rod outer segment disc membranes. *J. Mol. Biol.* 154:145–157.

Unger, V. M., P. A. Hargrave, J. M. Baldwin, and G. F. X. Schertler. 1997. Arrangement of rhodopsin transmembrane α-helices. *Nature*. 389: 203–206.

Varma, R., and S. Mayor. 1998. GPI-anchored proteins are organized in submicron domains at the cell surface. *Nature.* 394:798–801.

Welti, R., and M. Glaser. 1994. Lipid domains in model and biological membranes. *Chem. Phys. Lipids.* 73:121–137.

Williams, E. E., L. J. Jenski, and W. Stillwell. 1998. Docosahexaenoic acid (DHA) alters the structure and composition of membranous vesicles exfoliated from the surface of a murine leukemia cell line. *Biochim. Biophys. Acta.* 1371:351–362.

Zuvic-Butorac, M., P. Muller, T. Pomorski, J. Libera, A. Herrmannm, and M. Schara. 1999. Lipid domains in the exoplasmic and cytoplasmic leaflet of the human erythrocyte membrane: a spin label approach. *Eur. Biophys. J.* 28:302–311.